Eur Biophys J (2011) 40:1007–1012
DOI 10.1007/s00249-011-0714-3

BIOPHYSICS LETTER

# Combination of extended X-ray absorption fine structure spectroscopy with lipidic cubic phases for the study of cation binding in bacteriorhodopsin

**Alex Perálvarez-Marín · Francesc Sepulcre · Mercedes Márquez · Maria Grazia Proietti · Esteve Padrós**

Received: 20 October 2010 / Revised: 10 May 2011 / Accepted: 18 May 2011 / Published online: 12 June 2011


**Abstract** We have performed a quantitative X-ray absorption fine structure analysis of bacteriorhodopsin in purple membrane patches and in lipidic cubic phases regenerated with $Mn^{2+}$. Lipidic cubic phases and purple membrane results have been compared, demonstrating that the lipidic cubic phase process does not introduce relevant distortions in the local geometry of the cation binding sites. For both samples, we have observed similarities for $Mn^{2+}$ coordination in terms of type, number, and average distances of surrounding atoms, indicating a first coordination shell composed by 6 O atoms, and 3/4 C atoms located in the second coordination shell.

A. Perálvarez-Marín and F. Sepulcre contributed equally.

A. Perálvarez-Marín · M. Márquez · E. Padrós
Unitat de Biofísica, Departament de Bioquímica i de Biologia Molecular and Centre d'Estudis en Biofísica, Facultat de Medicina, Universitat Autònoma de Barcelona, 08193 Bellaterra, Spain

A. Perálvarez-Marín (✉)
Department of Molecular and Cell Biology, Harvard University, Northwest Building, 52 Oxford Street Room 311, Cambridge, MA 02138, USA
e-mail: peralvarezmarin@gmail.com

F. Sepulcre (✉)
Departament d'Enginyeria Agroalimentària i Biotecnologia, Universitat Politècnica de Catalunya, Campus del Baix Llobregat. Escola Superior d'Agricultura de Barcelona, C/Esteve Terradas 8, Castelldefels, 08860 Barcelona, Spain
e-mail: francesc.sepulcre@upc.edu

M. G. Proietti
Instituto de Ciencia de los Materiales de Aragón-Dep Física de la Materia Condensada, Facultad de Ciencias, CSIC-Universidad de Zaragoza, Zaragoza, Spain

**Keywords** Membrane protein · EXAFS · Cation binding · Bacteriorhodopsin · Lipidic cubic phase

## Introduction

Bacteriorhodopsin (BR) is the only protein found in the purple membrane (PM) of *Halobacterium salinarum*. PM is arranged as two-dimensional crystalline patches constituted by BR hexagonal lattices, where 75% of the weight corresponds to BR and the remaining 25% to phospho- and sulfolipids (Dracheva et al. 1996). BR has a retinal molecule covalently linked to Lys216 and functions as a light-driven proton pump, thus generating a proton gradient across the cell membrane, which is subsequently converted into chemical energy (Hirai and Subramaniam 2003; Lanyi 2001).

BR arranged in PM binds 4 mol $Ca^{2+}$ and 1 mol $Mg^{2+}$ per mole of chromoprotein (Kimura et al. 1984). The role of these cations has been proven relevant for the function of the protein. The location and some of the structural and functional features of these cations still need to be resolved (Duñach et al. 1986, 1988a, b, 1989; Sepulcre et al. 2005; Yang and el-Sayed 1995; Yoo et al. 1995; Zhang and el-Sayed 1993; Zhang et al. 1992, 1993; Eliash et al. 2001; Jonas and Ebrey 1991; Sepulcre et al. 1996, 2004, 2007; Tuzi et al. 1999; Wassenaar et al. 2009). Even though several three-dimensional (3-D) structures of BR have been published in recent years, none reports the presence of metal cations. This could be explained because they are in part or completely lost upon crystallization. In contrast, all of these 3-D structures show different Asp and Glu groups that in terms of geometry and bond distances are compatible with the presence of cation binding sites (Luecke et al. 1999). In an effort to understand the role of metal cations in

the BR function, the binding characteristics of these cations have been analyzed using different techniques. Regarding their location, both specific and nonspecific binding sites have been proposed. The specific sites have been suggested to be in (1) the retinal surroundings, which influences the state of protonation of Asp85 (i.e., the color of the pigment) (Jonas and Ebrey 1991; Sepulcre et al. 1996, 2004; Wassenaar et al. 2009; Zhang et al. 1992), (2) the cytoplasmic loop between helices F and G (Tuzi et al. 1999), and (3) in the proximities of Glu194/Glu204 in the extracellular side of the membrane (Eliash et al. 2001; Sanz et al. 2001; Sepulcre et al. 2007; Wassenaar et al. 2009). An alternative model suggested that the cations bind to the membrane surface and control the apparent p$K$ (p$K_a$) of Asp85 via the Gouy–Chapman model (Nollert et al. 1999). Nevertheless, the location of the metals and the associated conformational change due to cation binding remain unclear.

Extended X-ray absorption fine structure (EXAFS) spectroscopy has been proven to be an ideal tool to unravel cation interatomic distances and coordination numbers (Sepulcre et al. 1996, 2005; Jonas and Ebrey 1991; Sanz et al. 2001). The aims of the present study are the following: first, to test the diffusion of cations to specific binding sites in lipidic cubic phases (LCPs) of BR, and second, to check whether the incorporation of BR trimers into the lipidic cubic phases introduces distortions in the local geometry of the cation binding sites compared with BR in native PM suspensions. To answer these questions, we have regenerated BR LCPs with $Mn^{2+}$ and characterized the local environment by EXAFS spectroscopy.

## Materials and methods

Purple membranes from *Halobacterium salinarum* S9 strain were purified as previously described (Oesterhelt and Stoeckenius 1974).

Cations were removed from the PM by extensive dialysis using a cation-exchange Dowex AG-50W resin. In each case, a separate aliquot of deionized membrane was used for pH and spectroscopic controls to avoid any contamination. Regeneration was done at pH 7 by adding $Mn^{2+}$ at molar ratio of 5:1 ($Mn^{2+}$:BR) and checked by UV–Vis spectroscopy, verifying that the absorption band shifts were located, as expected, from 600 to 580–590 nm.

Solubilization and production of the lipidic cubic phases containing BR and monoolein (ratio 1:55 w/w) were performed as described in Facciotti et al. (2001). Tubes containing lipidic cubic phases were overlaid with an excess of 10 mM $MnCl_2$ solution (BR:$Mn^{2+}$ molar ratio at least 1:10) during a minimum of 10 days prior to EXAFS measurements. All the measured LCPs were exhaustively washed with distilled water before the measurements to remove $Mn^{2+}$ located on the LCP surface.

The X-ray absorption experiments were carried out at the ID26 beam line of the European Synchrotron Radiation Facility (ESRF). Measurements were carried out at 260 K in fluorescence mode at the Mn $k$-edge. The sample was moved automatically every five scans, and the results shown correspond to an average over about 10–12 h. Radiation damage or photoreduction can be excluded by checking the sample color changes associated to retinal bleaching. No alteration was observed for overall 5 min exposition. A monochromatic beam was obtained by means of a Si(111) double crystal, with energy resolution $\Delta E/E = 1.4 \times 10^{-4}$. The fluorescence signal at the Mn $k$-edge was detected by a multi-element silicon-drift solid-state detector.

Quantitative analysis of the EXAFS signal was performed by fitting the experimental spectra to theoretical signals calculated by means of phases and amplitudes generated by FEFF8 code (Ankudinov et al. 1998). The fitting procedure was carried out by means of the Ifeffit code (Newville 2001) implemented by the Artemis package (Ravel and Newville 2005).

One-shell and two-shell model clusters were used to obtain theoretical EXAFS signals for comparison with experimental EXAFS data. Information regarding the interactions of absorber (Mn)-scatters (O and C) was obtained by fitting the following equation to the EXAFS data:

$$\chi(k) = \sum_{s} \frac{N_s S_0^2 F_s(k)}{kR_s^2} \sin(2kR_s + \varphi_s(k)) \exp\left(-2\sigma_s^2 k^2\right) \exp\left(\frac{-2R_s}{\lambda(k)}\right), \quad (1)$$

where $F_s(k)$ is the effective scattering amplitude, $\varphi_s(k)$ is the effective scattering phase shift, and $S_0^2$ is the overall inelastic factor. $\sigma_s^2$ is the Debye–Waller term, $N_s$ is the number of scatters at distance $R_s$, and $\lambda(k)$ is the mean free path. The sum accounts for all scattering interactions. $k$, the photoelectron wavenumber of the ejected electrons, is defined by

$$k^2 = \frac{2m_e(E - E_0)}{\hbar^2}. \quad (2)$$

$E$ denotes the energy of the incident X-ray, and $E_0$ is the threshold energy for liberation of the photoelectron wave.

$E_0$ (origin value of the photoelectron energy) and the interatomic Mn–O and Mn–C distances ($R_s$) were allowed to vary freely to minimize the $\chi^2$ values ($R$-factor). The overall inelastic losses factor $S_0^2$ was fixed to a standard value of 0.8, and the EXAFS data were fitted in $k$-space in the range 2.5–9.4 $Å^{-1}$.

The Debye–Waller factors, which describe both static and dynamic fluctuations in interatomic distances, were calculated by the correlated Debye model implemented in IFFEFIT and described by Sevillano et al. (1979), in which the only two parameters required are the experimental temperature and the Debye temperature of the cluster ($\Theta_D$). The Debye temperatures ($\Theta_D$) of the different clusters were calculated according to

$$\Theta_D = \frac{h\upsilon}{K}, \quad (3)$$

where $h$ and $K$ are, respectively, the Planck constant and the Boltzmann constant, and $\upsilon$ is the experimental vibrational mode of Mn–carboxylate bonds. For simplicity, we have considered the average value of these frequency regions ($\upsilon = 600\ cm^{-1}$ for Mn–O bonds and $\upsilon = 1{,}750\ cm^{-1}$ for O–C bonds). This gives average values of $\Theta_{D(Mn-O)} = 936$ K and $\Theta_{D(O-C)} = 2{,}500$ K, respectively.

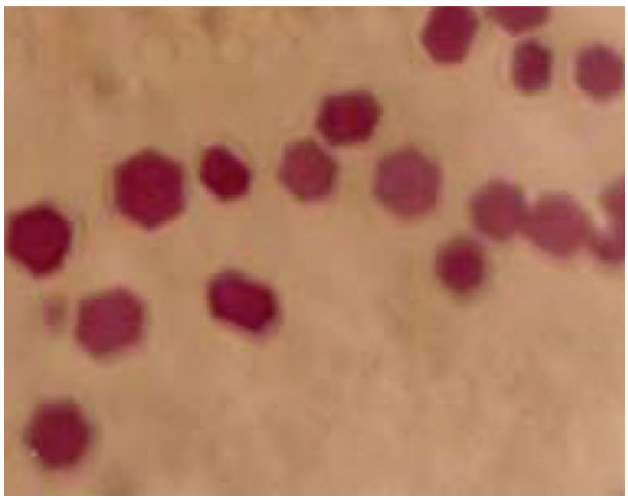

**Fig. 1** Lipidic cubic phases containing both ordered and unordered BR crystals (approx. 150 μm × 150 μm × 5 μm)

## Results

In the EXAFS technique, the $k$-space frequency, amplitude, and phase of the EXAFS oscillations are directly related to interatomic distances and the number and type of scatterers around the absorber. Due to its electronic properties and its similar behavior to physiological BR cations, $Mn^{2+}$ has been previously used to study the affinity binding sites in BR (Duñach et al. 1987; Sepulcre et al. 2005, 2007). LCPs containing BR crystals (with different size representation in the micrometer range, see Fig. 1) were incubated in the dark with a $Mn^{2+}$-containing buffer to fill the high- and medium-affinity binding sites of BR. The X-ray absorption Mn $k$-edges were obtained for BR LCPs, as well as for suspensions of deionized PM BR that were regenerated with 5 mol $Mn^{2+}$ per mol of BR (from now on called "PM suspension" sample). As a negative control, we also measured the EXAFS signal of LCPs not incubated in the buffer. No $Mn^{2+}$ $k$-edge EXAFS signal was observed in this case, indicating the absence of $Mn^{2+}$ inside the crystals (data not shown).

Background-subtracted EXAFS oscillations in $k$-space are presented in Fig. 2a. Each of the $\chi(k)$ spectra was characterized by a sine wave dominated by backscattering from first-shell atoms around $Mn^{2+}$ atom with the signal amplitude decreasing as $k$ increased. In comparison with PM suspensions, BR in LCPs showed a similar EXAFS curve with lower amplitude.

The Fourier transforms of the spectra are presented in Fig. 2b and 2c. A main peak centered at about 1.6 Å was observed for PM sample (thick grey line in Fig. 2b), whereas the main peak in the LCP sample was centered at 1.7 Å (thick grey line in Fig. 2c). The second/third peaks of the Fourier transforms are not clearly defined, indicating that both the

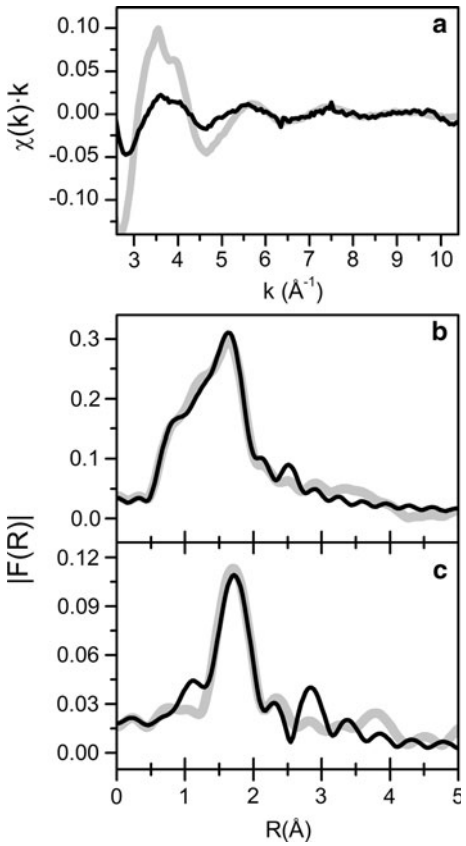


**Fig. 2** EXAFS analysis of BR in PM suspensions and in LCPs. **a** Experimental Mn $k$-edge EXAFS data for dark-adapted PM suspensions regenerated with $5Mn^{2+}$/BR (*grey line*) and dark-adapted BR in LCPs regenerated with $Mn^{2+}$ (*black line*). **b** Fourier transform of the EXAFS data corresponding to dark-adapted PM suspensions regenerated with $5Mn^{2+}$/BR (*grey line*) and the best fit (*black line*). **c** Fourier transform of the EXAFS data corresponding to dark-adapted BR in LCPs regenerated with $Mn^{2+}$ (*grey line*) and the best fit (*black line*)

number and the atomic weight of atoms in the second shell were small, but some similarity in the shape is observed for both samples. Peaks centered at about 2.2, 2.5, 2.9, and 3.5 Å were present in both samples (shifted to higher *R* values in the case of BR-LCP) with a similar relative intensity among them. This similarity is indicative of a similar local environment for $Mn^{2+}$ in the BR-LCP and 5 $Mn^{2+}$/BR samples.

To extract structural information of the $Mn^{2+}$ coordination to the protein, quantitative EXAFS analysis was performed. A model with the same average Mn–O distance for the six oxygen atoms was fitted to the EXAFS data, yielding poor results with a high *R*-factor value for both the PM suspensions and the LCPs (data not shown). Thus, we introduced some heterogeneity in this cluster by assigning different Mn–O distances for the different coordinated oxygen atoms (two oxygen shells). The results obtained are summarized in Table 1a. For the 5$Mn^{2+}$/BR sample, two Mn–O distances of 2.19 and 2.49 Å were found with coordination numbers of 4.2 and 1.8, respectively. The fitting of the two-oxygen-shell model to the LCPs data yielded again a high-*R*-factor value (i.e., a very poor fit).

In a second step, and to increase the fit quality, we introduced another shell formed by carbon atoms. The quantitative fit results obtained for this cluster are reported in Table 1b and shown in Figs. 2b and c (as a solid black line for PM suspensions and LCPs, respectively). Including an extra Mn–C shell improved the fitting in both PM suspensions and in LCPs, defining a six oxygen atom coordination number for $Mn^{2+}$.

We studied also the possibility that the cation binding occurred around P and/or S atoms from phospho- and sulfolipids of the PM. We have ruled out this possibility due to the very poor fitting results, in agreement with our previous work (Sepulcre et al. 2005). The possibility of Mn–Mn interactions due to cation aggregation or Mn crystallization was also discarded by comparing the theoretical EXAFS spectra of Mn–Mn and Mn–O-Mn (manganese hydroxide) with our experimental data. An intense peak at about 2.7–2.9 Å appeared in the Fourier transform, in contrast with the experimental results (data not shown) in all these theoretical models.

To summarize, the quantitative fit showed similarities for $Mn^{2+}$ coordination when bound to BR in both PM suspensions and LCPs. The best fitting was obtained when the model with two Mn–O shells was improved with a third C shell. This model explained the results better than $Mn^{2+}$ crystallization/aggregation processes or the coordination of the cations with the lipidic S and P groups.

## Discussion

The binding of cations to BR influences the protonation state of Asp85 and subsequently the proton transport function. In this sense, characterization of the cation binding sites in BR represents an important subject to understand this molecular mechanism, and also to understand the relationship between the structure of the protein and its function.

We present a direct comparison between BR samples in PMs and in LCPs. The experimental conditions and $Mn^{2+}$/BR ratio are easier to define in the PM membrane sample,

**Table 1** Parameters for manganese coordination in PM suspensions and in LCPs

| Sample | Ligand | *R* (Å) | *N* | $\sigma^2$ (Å$^2$ × $10^{-3}$) $\theta_D$(Mn–O) = 936 K, fix | $E_0$ (eV) | *R*-factor |
|---|---|---|---|---|---|---|
| (a) Mn–O fit model | | | | | | |
| PM suspensions regenerated with 5$Mn^{2+}$/BR | O1 | 2.19 | 4.2 | 2.8 | −6.69 | 0.035 |
| | O2 | 2.49 | 1.8 | 2.9 | | |
| BR in LPCs regenerated with $Mn^{2+}$ | | | | | | >1 |
| Sample | Ligand | *R* (Å) | *N* | $\sigma^2$ (Å$^2$ × $10^{-3}$) $\theta_D$(Mn–O) = 936 K, fix $\theta_D$(O–C) = 2,500 K, fix | $E_0$ (eV) | *R*-factor |
| (b) Mn–O–C fit model | | | | | | |
| PM suspensions regenerated with 5$Mn^{2+}$/BR | $O_1$ | 2.19 | 3.6 | 2.8 | −4.66 | 0.019 |
| | $O_2$ | 2.44 | 2.4 | 2.9 | −4.66 | |
| | C | 2.77 | 3.0 | 1.1 | −0.23 | |
| BR in LPCs regenerated with $Mn^{2+}$ | $O_1$ | 2.27 | 2.4 | 2.6 | −0.39 | 0.080 |
| | $O_2$ | 2.58 | 3.6 | 2.7 | −0.39 | |
| | C | 2.86 | 4.2 | 1.1 | −5.40 | |

Fit parameters corresponding to (a) the one-shell model formed by oxygen atoms and (b) the two-shell model including a second coordination shell formed by C atoms. $E_0$ and *R* were iterated ($S_0^2 = 0.8$)

whereas in the case of LCPs, it is difficult to define the amount of $Mn^{2+}$ diffusing to the protein. It should also be taken into account that the new interlayer contacts established through the loops BC and EF to form the LCP crystals (Belrhali et al. 1999) could influence the cation binding sites. These questions appear to be relevant in view of the use of LCPs to obtain BR structures. In this study we have gone one step further in the cation binding site characterization in BR: $Mn^{2+}$ is bound by two oxygen shells as first neighbors, followed by a carbon atom shell, as expected for a carboxylic acid. We had previously shown that after retinal depletion only one Mn–O distance is observed, indicating that a tertiary structure change leads to the disappearance of one of the specific cavities for $Mn^{2+}$ in the bleached BR PM (Sepulcre et al. 2005). In contrast, the existence of two different Mn–O distances and very similar values for the Debye–Waller parameters ($\sigma^2$) found for both samples studied here (BR in PM and BR in LCPs) indicates that the structure of BR that configures the cavities occupied by cations is conserved. LCPs were originally prepared using sodium phosphate buffer, thus we can speculate that there has been a substitution of monovalent $Na^{+}$ by divalent $Mn^{2+}$ after the incubation period, which confirms that the affinity for the conserved cavities is higher for divalent cations (Belrhali et al. 1999). Both the presence of cavities in PM suspensions and LCPs and the potential displacement of monovalent cations argue for the conservation and specificity of the cation binding sites of BR in LCPs.

**Acknowledgments** We acknowledge the European Synchrotron Radiation Facility for provision of synchrotron radiation facilities and we would like to thank Dr. Pieter Glatzel for assistance in using the ID26 beam line. This work was supported by a Dirección General de Investigación grant BFU2006-04656/BMC, BFU2009-08758, and a Marie Curie International Outgoing Fellowship to A.P.-M. within the 7th European Community Framework Programme (PIOF-GA-2009-237120).

## References

Ankudinov AL, Ravel B, Rehr JJ, Conradson SD (1998) Real-space multiple-scattering calculation and interpretation of X-ray-absorption near edge structure. Phys Rev B 58:7565–7576

Belrhali H, Nollert P, Royant A, Menzel C, Rosenbusch JP, Landau EM, Pebay-Peyroula E (1999) Protein, lipid and water organization in bacteriorhodopsin crystals: a molecular view of the purple membrane at 1.9 A resolution. Structure 7(8):909–917

Dracheva S, Bose S, Hendler RW (1996) Chemical and functional studies on the importance of purple membrane lipids in bacteriorhodopsin. Photocycle Behav 382(1–2):209–212

Duñach M, Seigneuret M, Rigaud JL, Padrós E (1986) The relationship between the chromophore moiety and the cation binding sites in bacteriorhodopsin. Biosci Rep 6(11):961–966

Duñach M, Seigneuret M, Riguad JL, Padrós E (1987) Characterization of the cation binding-sites of the purple membrane—electron-spin-resonance and flash-photolysis studies. Biochemistry 26(4):1179–1186

Duñach M, Padrós E, Seigneuret M, Rigaud JL (1988a) On the molecular mechanism of the blue to purple transition of bacteriorhodopsin. UV-difference spectroscopy and electron spin resonance studies. J Biol Chem 263(16):7555–7559

Duñach M, Seigneuret M, Rigaud JL, Padrós E (1988b) Influence of cations on the blue to purple transition of bacteriorhodopsin. Comparison of $Ca2^{+}$ and $Hg2^{+}$ binding and their effect on the surface potential. J Biol Chem 263(33):17378–17384

Duñach M, Padrós E, Muga A, Arrondo JL (1989) Fourier-transform infrared studies on cation binding to native and modified purple membranes. Biochemistry 28(22):8940–8945

Eliash T, Weiner L, Ottolenghi M, Sheves M (2001) Specific binding sites for cations in bacteriorhodopsin. Biophys J 81(2):1155–1162

Facciotti MT, Rouhani S, Burkard FT, Betancourt FM, Downing KH, Rose RB, McDermott G, Glaeser RM (2001) Structure of an early intermediate in the M-state phase of the bacteriorhodopsin photocycle. Biophys J 81(6):3442–3455

Hirai T, Subramaniam S (2003) Structural insights into the mechanism of proton pumping by bacteriorhodopsin. FEBS Lett 545(1):2–8

Jonas R, Ebrey TG (1991) Binding of a single divalent cation directly correlates with the blue-to-purple transition in bacteriorhodopsin. Proc Nat Acad Sci USA 88(1):149–153

Kimura Y, Ikegami A, Stoeckenius W (1984) Salt and pH-dependent changes of the purple membrane absorption spectrum. Photochem Photobiol 40(5):641–646

Lanyi JK (2001) X-ray crystallography of bacteriorhodopsin and its photointermediates: insights into the mechanism of proton transport. Biochemistry (Moscow) 66(11):1192–1196

Luecke H, Schobert B, Richter HT, Cartailler JP, Lanyi JK (1999) Structure of bacteriorhodopsin at 1.55 A resolution. J Mol Biol 291(4):899–911. doi:10.1006/jmbi.1999.3027

Newville M (2001) IFEFFIT: interactive XAFS analysis and FEFF fitting. J Synchrotron Radiat 8:3

Nollert P, Royant A, Pebay-Peyroula E, Landau EM (1999) Detergent-free membrane protein crystallization. FEBS Lett 457(2):205–208

Oesterhelt D, Stoeckenius W (1974) Isolation of the cell membrane of Halobacterium halobium and its fractionation into red and purple membrane. Methods Enzymol 31(Pt A):667–678

Ravel B, Newville M (2005) ATHENA, ARTHEMIS, HEPHAESTUS: data analysis for x-ray absorption spectroscopy using IFEFFIT. J Sybchrotron Radiat 12:537–541

Sanz C, Marquez M, Perálvarez A, Elouatik S, Sepulcre F, Querol E, Lazarova T, Padrós E (2001) Contribution of extracellular Glu residues to the structure and function of bacteriorhodopsin. Presence of specific cation-binding sites. J Biol Chem 276(44):40788–40794

Sepulcre F, Cladera J, Garcia J, Proietti MG, Torres J, Padrós E (1996) An extended x-ray absorption fine structure study of the high-affinity cation-binding site in the purple membrane. Biophys J 70(2):852–856

Sepulcre F, Proietti MG, Benfatto M, Della Longa S, Garcia J, Padrós E (2004) A quantitative XANES analysis of the calcium high-affinity binding site of the purple membrane. Biophys J 87(1):513–520

Sepulcre F, Proietti M, Benfatto M, Della Longa S, Garcia J, Padrós E (2005) An XAS study of the cation binding sites in the purple membrane of Halobacterium salinarum. Physica Scripta T115:855–858

Sepulcre F, Cordomi A, Proietti MG, Perez JJ, Garcia J, Querol E, Padrós E (2007) X-ray absorption and molecular dynamics study

of cation binding sites in the purple membrane. Proteins 67(2):360–374

Sevillano E, Meuth H, Rehr JJ (1979) Extended X-Ray Absorption Fine-Structure Debye-Waller Factors. 1 Monatomic crystals. Phys Rev B 20(12):4908–4911

Tuzi S, Yamaguchi S, Tanio M, Konishi H, Inoue S, Naito A, Needleman R, Lanyi JK, SaitÃ' H (1999) Location of a cation-binding site in the loop between helices F and G of bacteriorhodopsin as studied by 13C NMR. Biophys J 76(3):1523–1531

Wassenaar TA, Daura X, Padrós E, Mark AE (2009) Calcium binding to the purple membrane: A molecular dynamics study. Prot-Struct Func Bioinfo 74(3):669–681

Yang D, el-Sayed MA (1995) The $Ca2^{+}$ binding to deionized monomerized and to retinal removed bacteriorhodopsin. Biophys J 69(5):2056–2059

Yoo SK, Awad ES, Elsayed MA (1995) Comparison between the Binding of $Ca2^{+}$ and $Mg2^{+}$ to the 2 High-Affinity Sites of Bacteriorhodopsin. J Phys Chem 99(29):11600–11604

Zhang NY, el-Sayed MA (1993) The C-terminus and the $Ca2^{+}$ low-affinity binding sites in bacteriorhodopsin. Biochemistry 32(51):14173–14175

Zhang YN, Sweetman LL, Awad ES, El-Sayed MA (1992) Nature of the individual Ca binding sites in Ca-regenerated bacteriorhodopsin. Biophys J 61(5):1201–1206

Zhang YN, el-Sayed MA, Bonet ML, Lanyi JK, Chang M, Ni B, Needleman R (1993) Effects of genetic replacements of charged and H-bonding residues in the retinal pocket on $Ca2^{+}$ binding to deionized bacteriorhodopsin. Proc Natl Acad Sci USA 90(4):1445–1449